Society For Biomaterials

Toxicity evaluation of high-fluorescent rare-earth metal nanoparticles for bioimaging applications

Luis Hernandez-Adame,[1] Nancy Cortez-Espinosa,[2] Diana P. Portales-Pérez,[2] Claudia Castillo,[3] Wayne Zhao,[4] Zaida N. Juarez,[5] Luis R. Hernandez,[6] Horacio Bach,[4] Gabriela Palestino[1]

[1]Laboratory of BioPolymers and Nanostructrures, Faculty of Chemical Sciences, Universidad Autónoma de San Luis Potosí, CP 78210, San Luis Potosí, S.L.P., México
[2]Laboratory of Immunology and Molecular and Celullar Biology, Faculty of Chemical Sciences, Universidad Autónoma de San Luis Potosí, CP 78210, San Luis Potosí, S.L.P., México
[3]Bioquemistry, Faculty of Medicine, Universidad Autónoma de San Luis Potosí, CP 78210, San Luis Potosí, S.L.P., México
[4]Division of Infectious Diseases, Faculty of Medicine, University of British Columbia, Vancouver, BC V6H 3Z6, Canada
[5]Department of Chemical Engineering, Food and Environmental, Universidad de las Américas Puebla, 72810 San Andrés Cholula, Puebla, México
[6]Department of Chemical and Biological Sciences, Universidad de las Américas Puebla, 72810 San Andrés Cholula, Puebla, México

Received 23 July 2015; revised 18 October 2015; accepted 9 November 2015
Published online 00 Month 2015 in Wiley Online Library (wileyonlinelibrary.com). DOI: 10.1002/jbm.b.33577

Abstract: Research on nanometer-sized luminescent semiconductors and their biological applications in detectors and contrasting agents is an emergent field in nanotechnology. When new nanosize technologies are developed for human health applications, their interaction with biological systems should be studied in depth. Rare-earth elements are used in medical and industrial applications, but their toxic effects are not known. In this work, the biological interaction between terbium-doped gadolinium oxysulfide nanoparticles (GOSNPs) with human peripheral blood mononuclear cells (PBMC), human-derived macrophages (THP-1), and human cervical carcinoma cell (HeLa) were evaluated. The GOSNPs were synthetized using a hydrothermal method to obtain monodisperse nanoparticles with an average size of 91 ± 9 nm. Characterization techniques showed the hexagonal phase of the $Gd_2O_2S{:}Tb^{3+}$ free of impurities, and a strong green emission at $\lambda_{emi} = 544$ nm produced by Tb^{3+} was observed. Toxic effects of GOSNPs were evaluated using cell viability, apoptosis, cell-cycle progression, and immunological response techniques. In addition, an *Artemia* model was used to assess the toxicity *in vivo*. Results indicated cell apoptosis in both types of cells with less sensitivity for PBMC cells compared to HeLa cells. In addition, no toxic effects were observed in the *in vivo* model of *Artemia*. Moreover, GOSNPs significantly reduced the activation and cell-cycle progression of PBMC and HeLa cells, respectively. Interestingly, an increase in proinflammatory cytokines was not observed. Our data suggest that fluorescence applications of GOSNPs for biolabeling are not toxic in primary immune cells and they may have an immunomodulatory effect. © 2015 Wiley Periodicals, Inc. J Biomed Mater Res Part B: Appl Biomater 00B: 000–000, 2015.

Key Words: oxysulfides, biological cells, toxicity, immunomodulatory effect

How to cite this article: Hernandez-Adame L, Cortez-Espinosa N, Portales-Pérez DP, Castillo C, Zhao W, Juarez ZN, Hernandez LR, Bach H, Palestino G. 2015. Toxicity evaluation of high-fluorescent rare-earth metal nanoparticles for bioimaging applications. J Biomed Mater Res Part B 2015:00B:000–000.

INTRODUCTION

Over the last few decades, the use of nanomaterials in biomedical applications has been extensively studied due to their distinctive chemical and physical properties.[1] Particularly, in the area of biosensing, quantum dots (QDs), Au, Ag, Pt, Cu, and Gd nanoparticles (NPs) have been studied to develop detection devices exploiting magnetic and/or optical properties of these active elements as signal transducers.[2–4] However, recent works have shown that certain nonlinear effects related to the optical properties of these elements limit their luminescence response.[5,6] Moreover, since these elements possess potential cytotoxicity for *in vivo* applications, their use in the biomedical field has been restricted. Although this problem can be partially solved by surface functionalization of the NPs, the procedures to achieve such functionalization often require complex strategies.[7–9]

Previous studies have reported the use of dye-doped silica particles for tracking cells, with minimum damage,[10] but these particles showed poor stability and low-optical response, mainly due to photobleaching that occurs within a few seconds under standard conditions of illumination.[7,11] In this context, doped rare-earth oxysulfides (RE_2O_2S) are emerging NPs as

Correspondence to: G. Palestino, Ph.D.; e-mail: palestinogabriela@fcq.uaslp.mx
Contract grant sponsor: CONACYT Projects CB-153161, and Infrastructure 225843; FAI C12-FAI-03-94.94

potential candidates to solve this problem, mainly due to their (1) high photoluminescence, (2) high photostability, (3) blinking absence, (4) extremely narrow emission lines, (5) large stokes shifts, and (6) long lifetimes.[12,13]

One of the most interesting RE_2O_2S is the terbium-doped gadolinium oxysulfide NPs—$Gd_2O_2S:Tb^{3+}$ (GOSNPs), which is a photoluminescent phosphor used as an optical device in solid-state lasers, screens for X-ray detection, optical amplifiers, and color displays.[14–16]. GOSNPs are characterized by their high density (7.44 g/cm^{-3}), which improves UV–photon absorption. In addition, they possess a high intrinsic conversion efficiency (~27%) that results in a strong visible light output, a desired characteristic for such phosphors.[17] These characteristics indicate that GOSNPs might be a better option for biolabeling compared with organic dyes, QDs, or lanthanide metallic oxides such as Gd_2O_3 or $Gd_2O_3:Tb^{3+}$.

In a previous report, we demonstrated that the main advantage of the GOSNPs is their strong emission intensity (70-fold higher as compared to oxides),[18] which highlights the excellent optical properties of these NPs. These properties can be used to enhance the sensitivity and quality of optical imaging or detection. However, the use of these materials for biomedical applications requires in-depth analysis of their toxicity and biocompatibility. Some studies on Gd_2O_3 particles have shown low cytotoxicity of the rare-earth oxides[6]; nevertheless, to our knowledge, there has been no study on the biological effects of rare-earth oxysulfides. In this regard, we have produced GOSNPs with a spherical shape and have evaluated their impact on cellular biological functions, specifically their interaction with cells of the immune system.

MATERIALS AND METHODS

GOSNPs synthesis and characterization

In order to obtain the GOSNP samples, the methodology previously reported by our group was employed.[18] All reagents were of the highest possible quality and were used with no further purification (Sigma-Aldrich, St. Louis, MO). NP synthesis was carried out in three stages: (1) growth of hydroxycarbonate NPs, (2) formation of oxide crystalline phase ($Gd_2O_3:Tb^{3+}$), and (3) the production of the oxysulfide NPs ($Gd_2O_2S:Tb^{3+}$) through a sulfidation process.[18]

Physicochemical characterization of GOSNP

The morphology and particle size of the NPs were analyzed using transmission electron microscopy (TEM) with a Jem Joel 1230 instrument (Joel, Japan) operated at 200 kV. The samples were prepared after suspending the GOSNPs in acetone prior to being deposited on the grid. Chemical analysis was determined by Fourier Transform Infrared Spectroscopy (FTIR) by using a Bruker Vector 22 and Agilent 660 (Bruker Instruments, Billerica, MA, USA) instruments coupled with a diamond crystal ATR accessories. The samples were dried and prepared as a powder. Spectra were recorded in the range of 4000–400 cm^{-1}. The crystallographic phase was determined by wide-angle X-ray diffraction (WAXD) technique. The measurements were performed with a small amount of GOSNPs in a PANalytical diffractometer model Xpert pro (PANalytical, The Netherlands). The samples were irradiated with Cu Kα_1 ($\lambda = 1.540598$ nm) and Cu Kα_2 ($\lambda = 1.5444$ nm) radiation and the diffractograms were recorded from 20° to 70° (2θ) at a step size of 0.016°. The photoluminescence (PL) properties were evaluated in solid form at room temperature using a Horiba Join-Yvon spectrometer model NanoLog (Horiba Jobin Yvon, France). GOSNPs (100 mg) were pelleted by applying a pressure of 3 tons for 25 min. The emission spectra were recorded using a Xenon lamp with $\lambda_{exc} = 292$ nm. In order to determine the stability of the GOSNPs in physiological conditions, the ζ-potential was measured in three different solutions: pH 7.4 phosphate-buffered saline (PBS), a cell culture media such as RPMI-1640 (GIBCO, Life Technologies, MD, USA), and DMEM (Sigma, St. Louis, MO). ζ-potential measurements were carried out using the Dynamic Light Scattering technique (DLS) using a Nano Zetasizer (Malvern, UK). An aqueous GOSNP suspension [2% (w/v)] was prepared using the colloidal vibration method as published.[19] This suspension was diluted 1:2 either with PBS, RPMI-1640, or DMEM. Measurements were performed with an equilibration temperature of 25°C for 1 min and repeated at least 3 times. For a correct optical model, refractive index (Ri) and viscosity (η) values of the media were obtained from the literature. Ri of 1.330 and 1.345 and η of 1.4 and 0.748 mPa were used for RPMI and DMEM, respectively.[20–22]

Cell cultures

Peripheral blood mononuclear cells (PBMC) from volunteers were used in this study. An informed consent and ethical statement on the use of human material were obtained from the ethical committee of the Universidad Autónoma de San Luis Potosí (number: 10–11). PBMC from healthy subjects were isolated using a Ficoll–Hypaque density gradient (Sigma). These cells were cultured in 48-well tissue culture plates using RPMI-1640 medium (Gibco, Thermo Fisher, MA), supplemented with L-glutamine (Sigma), 10% fetal bovine serum (Gibco), 100 U/mL penicillin, and 100 μg/mL streptomycin (Sigma). Human cervical carcinoma cells (HeLa) were cultured in DMEM medium and used for up to six passages according to the manufacturer's instructions. Human-derived monocytes THP-1 (ATCC TIB-202) were cultured in RPMI medium supplemented with the same reagents used with DMEM. Macrophages were obtained by overnight differentiation of monocytes using phorbol 12-myristate 13-acetate (PMA, Sigma). Macrophages were dispensed at a final density of 5×10^4 cells in a 96-well plate. All cells were incubated at 37°C in a humidified incubator supplemented with 5% CO_2.

GOSNPs internalization

The internalization of GOSNPs was calculated as the percentage of cells that increased their side scattering light (SSC) in the flow cytometer and according to published protocols.[23] In brief, the number of cells in culture medium (P2) (without GOSNPs) was gated and considered as 100%. Then, the percentage of cells showing a change in the SSC was measured and defined as P1. The percentage of cells that internalized GOSNPs was calculated as follows: $100\% - (P1 \times 100/P2)$. Experiments were performed in triplicate.

Treatment of cells with GOSNPs

Cells were treated for 24, 48, and 72 h with different GOSNP concentrations. A stock solution of 1 mg/mL of GOSNPs was prepared in PBS and sonicated at room temperature for 30 min to allow dispersion. Cells were exposed to final concentrations of 125, 250, or 500 μg/mL after diluting the GOSNPs in culture medium. PBS was used as a negative control, whereas PMA (50 ng/mL) or anti-CD3 and anti-CD28 (5 μg/mL, eBioscience, San Diego, CA, USA) were used as positive controls.

Cells were cultured in the presence or absence of different concentrations of GOSNPs for 24, 48, and 72 h. After the treatment, the metabolic activity of THP1 cells was assessed by MTS (Promega, Madison, WI, USA) and according to the manufacturer's instructions, whereas PBMC and HeLa cells were trypsinized and membrane cytotoxicity was measured by propidium iodide (PI) (Sigma) using flow cytometry (FACSCanto flow cytometer, Becton-Dikinson, Franklin Lakes, NJ, USA) using the FACSDiva software. Additionally, cell viability was analyzed using the trypan blue (Sigma) exclusion assay and conventional light microscopy under identical conditions as previously mentioned for the cytotoxicity assays.

Activation-induced CD69 expression and cell cycle

To evaluate activation status, PBMC were stimulated with PMA or anti-CD3/CD28 with or without the indicated GOSNPs concentrations. After each incubation time, cells were immunostained with the activation antigen CD69 (anti-CD69-phycoerytrin, eBioscience, San Diego, CA, USA) or the isotype antibody (eBioscience) as a control and analyzed using flow cytometry. Results were expressed as the percentage of CD69-positive cells. For the cell-cycle assay, PBMC were stimulated with 50 ng/mL PMA and 0.5 μg/mL ionomycin or anti-CD3/CD28 with or without GOSNP concentrations for 24, 48, and 72 h. Then, the cell nuclei were stained using PI in sodium citrate (Sigma) and 0.3% Triton X-100 (Sigma), and the nuclear DNA content was analyzed using flow cytometry. Results were expressed as the percentage of cells corresponding to the G0/G1 (normal diploid DNA phase), the synthesis (S), and the G2/M (mitosis phase) phases of the cell cycle. Additionally, HeLa cells were used and cultured only in the presence of GOSNPs for the same period of time described for PBMC.

Flow cytometry and confocal microscopy

Flow cytometry was used to evaluate the cellular uptake of PBMC or HeLa cells when they were exposed to GOSNPs. Both cells were separately incubated with GOSNPs at 125, 250, or 500 μg/mL, and exposed for 12, 24, and 48 h. Cells that were incubated in medium alone were used as negative control (RPMI-1640 culture medium for PBMC and DMEM culture medium for HeLa cells). For the uptake analysis, detection of the cells was based on a scatter plot. Then, the distinctive scatter characteristics of each cell were accounted for by the difference in the refractiveness of cellular components; for example, nucleus, vesicles, and granules. Two types of scattering were simultaneously used for this purpose: (1) forward light scattering (FLS), which is related to the cell size, and (2) side scattering (SS), which is related to the cell complexity. This analysis was made in the same FACS Canto flow cytometer (Becton-Dikinson) as mentioned above using the Cell Quest software. In parallel, confocal microscopy was used to evaluate the fluorescence and localization of NPs inside HeLa cells. These cells were plated onto culture dishes containing a sterile glass cover slip at a density of 5×10^5 cells/mL. Cells were allowed to adhere for 48 h. Then, GOSNPs were added to the cultures at 125, 250, or 500 μg/mL, and exposed for 6, 8, 10, 12, and 24 h. Samples were processed by removing the culture medium and applying consecutive washes with PBS solution. Confocal images were obtained after fixing the cells with 4% paraformaldehyde (Sigma Aldrich, St. Louis, MO, USA) for 10 min. To improve the image contrast, nuclei were stained with DAPI (1:500, Sigma). Cells were imaged using a Zeiss LSM 510 Meta confocal microscope (Carl Zeiss Inc., Thornwood, NY, USA). The images were obtained at an excitation wavelength of 313 nm and filtered in the emission range of 540–620 nm.

Apoptosis measurement

The effect of GOSNPs on apoptosis was analyzed using the annexin-V-FITC apoptosis detection kit according to the manufactures instructions (eBioscience). The PBMC were cultured in 96-well tissue culture plates using RPMI-1640 medium (Gibco), supplemented with L-glutamine (Sigma), 10% fetal bovine serum (Gibco), 100 U/mL penicillin, and 100 μg/mL streptomycin (Sigma). Cells were incubated with or without GOSNPs to final concentrations of 30, 60, 125, 250, or 500 μg/mL for 12, 24, and 48 h. Then, cell suspension was incubated with annexin-V-FITC and PI for 20 min to 4°C and tested for apoptosis and necrosis by flow cytometry.

Immune response

The secretion of the proinflammatory cytokines interleukin 6 (IL-6) and tumor necrosis factor-α (TNFα) was determined in the supernatant of macrophages (THP-1) after exposure to the NPs at concentrations varying between 0.5 and 50 μg/mL. In brief, 5×10^4 cells were differentiated using PMA as detailed above and exposed to the NPs for 24 h. Supernatants were collected and subjected to measurement of the cytokines using commercial kits (R&D, Minneapolis, MN, USA) according to the manufacturer's instructions. Untreated cells were used as negative control, whereas cells treated with lipopolysaccharide (100 ng/mL, Sigma) were used as positive control.

In vivo toxicity using the Artemia model

Encysted eggs of *Artemia* spp. (Azul, Mexico) were hatched in artificial seawater (Red Sea Fish Pharm, Israel), prepared with 30 g of commercial sea salt per liter of distilled water, and incubated at 25°C and using a photoperiod of 12 h. A total of 10 nauplii of 24 h old were used for the bioassay after their transfer to assay tubes of 10 mL borosilicate glass (Kimax, Kimble Chase, NJ, USA) using a pipette Pasteur. Nauplii were incubated with NPs at final concentrations of 5, 25, 50, 100, 250, 500, and 1000 μg/mL for 72 h. Distilled water was used as negative control, while potassium dichromate (Sigma) as a

positive control. Toxicity was estimated by calculating the LC_{50} determined after the 72 h incubation period. Nauplii were considered dead when movement was not detected after 10 s of observation. All the experiments were performed in triplicate. LC_{50} were calculated by using Probit analysis with a 95% confidence using Statgraphics Centurion XVI v. 16.2.04 (StatPoint Technologies, VA, USA).

Statistical analyses

Data were presented as the mean ± standard deviation (SD) of the percentage of positive cells. GraphPad Prism v.5 (GraphPad Software Inc, San Diego, CA, USA) was used for statistical analysis. Data distribution was determined using the Kolmogorov–Smirnov test. For the evaluation of significance among the groups, the ANOVA test with a Tukey post-hoc analyses was used. Differences among the groups were considered statistically significant at p values <0.05.

RESULTS

Characterization of GOSNPs

The shape and size of GOSNPs were characterized using TEM [Figure 1(A)]. Image showed spherical and well-dispersed GOSNPs with a homogenous size distribution of 91 ± 9 nm [Figure 1(A-I,A-II)].

The progress of surface chemistry changes of GOSNPs was monitored by FTIR [Figure 1(B)]. This analysis was essential to demonstrate that the high temperature used during the annealing process in NP fabrication was enough to remove all the residual chemical precursors. IR spectra showed that during the sulfidation process, the hydroxycarbonate groups (OH and CO_3^2) [Figure 1(B-III)] were eliminated rendering only the oxysulfides [Figure 1(B-IV)]. From a chemical point of view, these results suggest that after thermal treatments, the particle surface is free of organic functional groups or impurities.[18] To confirm the formation of a crystalline structure, hydroxycarbonate- and GOS-NPs were analyzed by WAXD technique. Diffractogram inspection in Figure 1(C) showed an undefined and amorphous pattern in the hydroxycarbonate NPs [Figure 1(C-V)], indicating that the material was formed before any thermal treatment. In contrast, GOSNPs diffraction pattern [Figure 1(C-VI)] showed

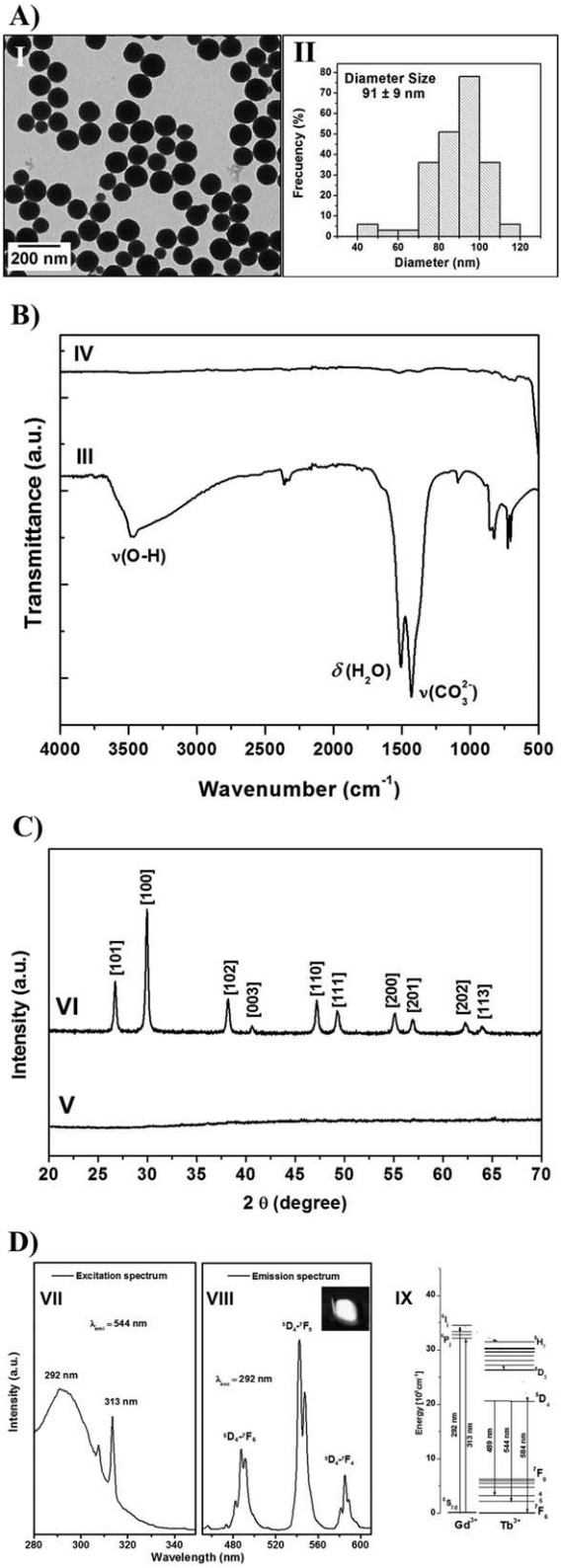

FIGURE 1. (A) Morphological analysis of GOSNPs. I. TEM image of GOSNP nanoparticles produced by hydrothermal method showing homogeneous and well-defined spherical nanoparticles. II. Size distribution histogram shows an average particle size of 91 ± 9 nm (TEM images were analyzed by using the Image J software). (B) Surface chemistry of GOSNPs at different steps of synthesis. III. FTIR spectrum of hydroxycarbonates nanoparticles showing the vibration modes of the organic precursors (CO_3^{2-}, OH), which confirm that the nanoparticles are made of hydrated gadolinium-terbium carbonates. IV. After the sulfidation reaction, FTIR spectrum shows the absence of organic vibrations, suggesting that the surface of the crystalline hexagonal lattice is free of organic groups. (C) Diffractograms of the hydroxycarbonate and oxysulfide nanoparticles. V. The diffractogram obtained in the first synthesis stage shows the amorphous phase of the hydroxycarbonates nanoparticles (no peaks are observed). VI. The diffractogram obtained after the sulfidation reaction at 900°C shows the well-defined hexagonal diffraction pattern of GOSNPs characteristic of oxysulfide hexagonal crystalline structure (card JCPDS 26-1422). Additional peaks were not observed denoting a high purity of the synthetized material. (D) Optical characterization of the GOSNPs at room temperature. VII. The excitation spectrum centered at the band emission of 544 nm. VIII. The emission spectrum with $\lambda_{exc} = 292$ nm and photograph of the real emission seen with the naked eye. IX. The energy level diagram and the electronic transitions involved in photoluminescence phenomenon.

TABLE I. ζ-Potential Values of the GOSNPs

Solution	ζ-potential of GOSNPs (mV)
Phosphate buffer	−17.4
RPMI 1640	−24.5
DMEM	−6.73

well-defined sharp peaks, which match perfectly with the reported hexagonal crystalline structure of $Gd_2O_2S{:}Tb^{3+}$ (card JCPDS 26-1422). It is important to emphasize that no additional peaks were observed in the diffractogram of GOSNPs, which confirms that the hydroxycarbonate precursors were converted to oxysulfide during the sulfidation process, validating the FTIR results. The stability of the GOSNPs in different media was determined by measuring ζ-potential. It was found that the ζ-potential of the particles in all cases was negative (Table I).

Optical properties

Excitation and emission spectra of GOSNPs are shown in Figure 1(D). In the case of the excitation spectrum [Figure 1(D-VII)], two peaks at 292 (most intense) and 313 nm were observed. These peaks are attributed to the electronic transition in the forbidden state f → f of Gd^{3+} ions from the fundamental state $^8S_{7/2}$ at the $6I_J$ and ^6P_J energetic levels,[24] respectively [Figure 1(D-IX)]. It is important to point out that an intense visible emission was observed even with naked eyes [Figure 1(D-VIII), inset].

Particle internalization

As demonstrated above, the remarkable optical properties of GOSNPs make them suitable for biomedical applications (biolabeling or bioimaging). To obtain information about the grade of biocompatibility and cytotoxicity of this material, a biological response was studied using PBMC and HeLa cells exposed to GOSNPs. We chose to study PBMC because NPs entering the bloodstream will encounter these cells. On the other hand, HeLa cells were used to obtain additional information to compare normal and immortalized cells.

The grade of internalization of PBMC [Figure 2(B-D)] and HeLa cells [Figure 2(F-H) and Table II] when exposed to GOSNPs for 24 [Figure 2(A–H)], 48, and 72 h (data no shown), was observed and compared with control cells [Figure 2(A,E)], which were incubated only in culture medium. We found that the uptake of GOSNPs in PBMC varies in a dose-dependent manner; therefore, cells treated with the highest NPs concentration (500 μg/mL) produced the highest light scatter points of dispersion [Figure 2(D)]. This concentration-dependent behavior was not observed when HeLa cells were assessed [Figure 2(F–H)].

GOSNPs internalization was confirmed using confocal fluorescence microscopy only in HeLa cells. The images displayed in the Figure 2(I–K) were obtained under an excitation wavelength of 313 nm and filtered in the emission range of 540–620 nm.

Cytotoxicity of GOSNPs

The cytotoxicity of GOSNPs and cell viability were assessed using annexin-V/PI and trypan blue dye, respectively. The dye exclusion trypan blue did not show differences in all of the GOSNPs concentrations, either PBMC or HeLa cells (Figure S1). Since both methods do not assess cell damage, a staining with PI was used. In this case, it was observed that after 24 h of incubation, the GOSNPs induced apoptosis in the HeLa cells in a dose-dependent manner [Figure 3(A)]. It is interesting to notice that under these conditions, the cytotoxicity of GOSNPs seems to be more important for cancer cells with higher percentages of positive cells for the IP (range: 2–13%) than the PBMC (1–3.5%). The same analysis was performed with cells treated with GOSNPs at 48 and 72 h. Nevertheless, cytotoxicity of GOSNPs was not observed at 48 h for any GOSNP concentration compared to the control condition in both types of cells. However at 72 h, the highest concentration of GOSNPs in PBMC and the lowest concentration of GOSNPs tested in HeLa showed significantly increased apoptosis compared with the control. However, the percentage of apoptosis induced by GOSNP is more evident in HeLa cells. The other conditions were similar between the control cells and the GOSNP-treated cells.

In addition to the cytotoxicity assays, we included lower GOSNPs concentrations and lower incubation times in cultures of PBMC [Figure 3(B–D)]. A high background of positive cells with annexin-V (early apoptosis) at 12 and 24 h of incubation was detected. We did not find a clear effect of GOSNPs in PBMC between incubation times or concentrations tested in double-positive cells to annexin-V+/IP+. On the other hand, the toxicity of the GOSNPs on *Artemia* spp. was also assayed. No mortality was observed in the first 24 h, and an LC_{50} of 1.547 μg/mL was calculated at 72 h.

Immunomodulatory effect of GOSNPs

To further explore the effect of GOSNPs on immune cells, the activation status of PBMC in the presence of GOSNPs was also evaluated. GOSNP-treated cells tended to have lower CD69 expression in a dose-dependent manner compared to control cells (Figure 4). This lower expression significantly diminished at 72 h when cells were treated with 500 μg/mL GOSNPs. However, this effect was not observed at the 48 h interval for the same concentration. In addition, when the cells were stimulated with anti-CD3 and anti-CD28 antibodies (anti-CD3/CD28) in the presence of GOSNPs, the percentage of CD69-positive cells was significantly diminished compared with cells that were only treated with anti-CD3/CD28. Interestingly, when GOSNPs were exposed to THP-1 cells, no secretion of proinflammatory cytokines was measured, suggesting that these NPs are not able to elicit an inflammatory response in macrophages.

Alternatively, we evaluated the effect of GOSNPs on the cell cycle of PBMC. Cell-cycle progression was not significantly affected by the GOSNP concentrations used or by the presence of PMA-ionomycin. Similar cell proportions in G0/G1, S, and G2/M phases of the cell cycle were detected at 24 (data not shown), 48, and 72 h [Figure 5(A–C)]. However, the induction of the cell cycle through stimulation with

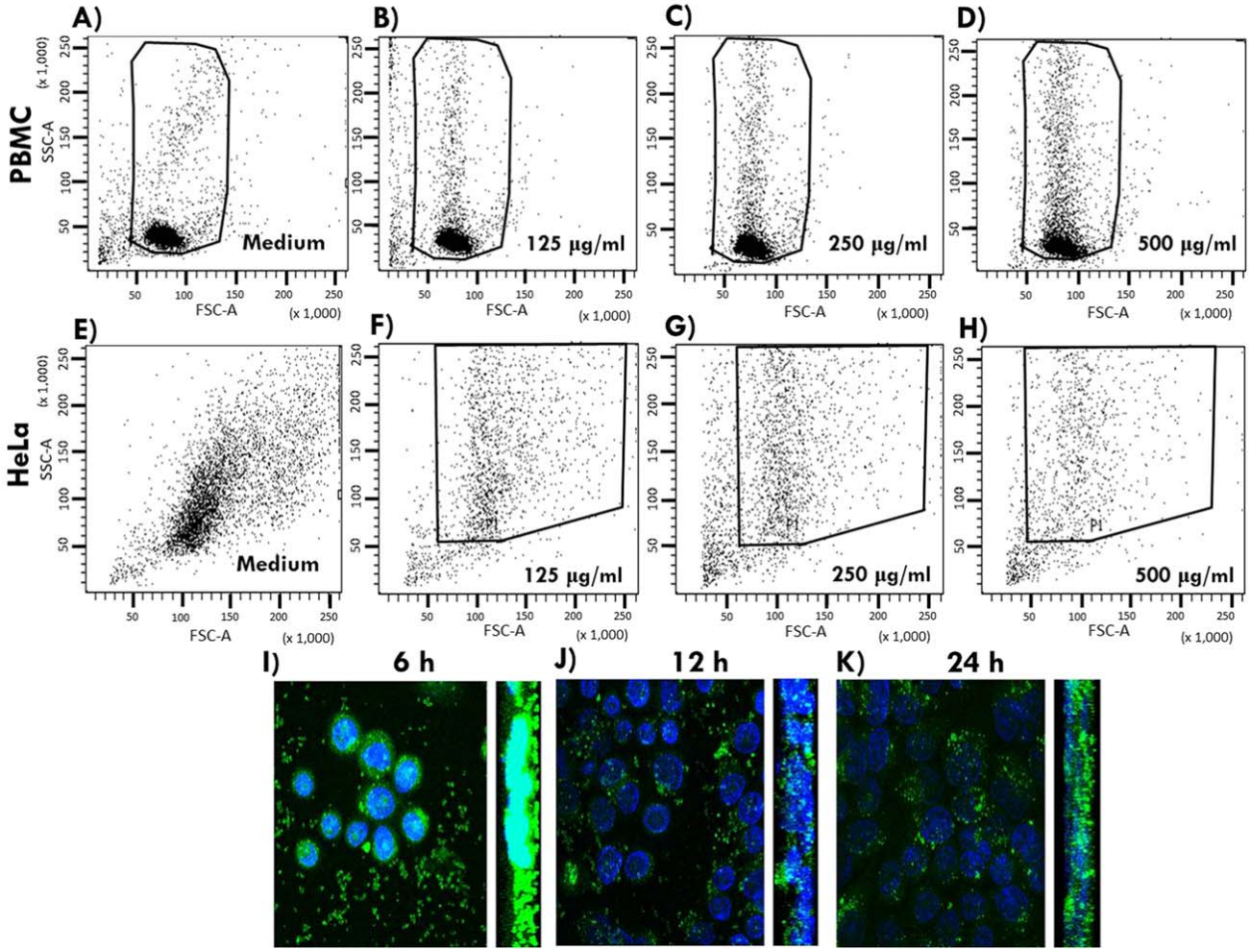

FIGURE 2. Cellular uptake of GOSNPs. Flow cytometry was used to evaluate the internalization of GOSNPs in the PBMC and HeLa cells at 24 h. The side scatter parameter was used to determine the uptake of the GOSNPs in the PBMC (Figures B–D) and in the HeLa cells (Figures F–H); and compared to the side scatter of the control cells (culture medium Figures A, E). The internalization of GOSNPs was calculated as the percentage of cells that increased their side scattering light (SSC). The number of cells in culture medium (P2) (without GOSNPs) was gated and considered as the 100%. The percentage of cells showing a change in the SSC was measured and defined as P1. The percentage of cells that internalized GOSNPs was calculated as follows: 100% − (P1 × 100/P2). [mt]20,000 cells were counted in each experiment. Positive cells for the uptake of GOSNPs were marked with a gate on each histogram. In addition, confocal microscopy was used to evaluate the fluorescence and localization of NPs inside HeLa cells as shown in the sagittal slide of Figures I–K. These cells were plated onto culture dishes containing a sterile glass cover slip at a density of 5×10^5 cells/mL. Cells were allowed to adhere for 48 h. Then, GOSNPs were added to the cultures at 250 µg/mL, and exposed for 6, 12, and 24 h. Samples were processed by removing the culture medium and applying consecutive washes with PBS (3×). Confocal images were obtained after fixing the cells with 4% paraformaldehyde for 10 min. To improve the image contrast, nuclei were stained with DAPI.

anti-CD3/CD28 resulted in a diminished proportion of S and G2/M cells exposed to GOSNPs in comparison with the cells that were only treated with anti-CD3/CD28 [Figure 5(B,C)]. When HeLa cells were tested, their cell-cycle progression was directly affected by GOSNPs in the absence of other stimuli. Different concentrations of GOSNPs resulted in a diminished proportion of G2/M cells at 48 and 72 h compared to the control cells [Figure 5(D–F)].

TABLE II. Percentage of GOSNP Internalization

		GOSNP Concentration (µg/mL)		
Cell Type	Time (h)	125 (%)	250 (%)	500 (%)
PBMC	24	85.37	69.08	53.51
	48	57.03	68.98	80.79
	72	63.08	72.42	82.28
HeLa	24	83.55	87.10	93.20
	48	85.15	89.57	94.75
	72	81.38	83.9	93.8

DISCUSSION

The detection of biomolecules is essential for many applications in biomedicine. However, these applications are often constrained by the available probes, whose optical properties may limit imaging possibilities. In this regard, the design of new nanomaterials represents an opportunity for medical applications. Here, we have studied the optical properties of GOSNPs for a potential role in biolabeling in both *in vitro* and *in vivo* systems. Unlike dyes and QDs,

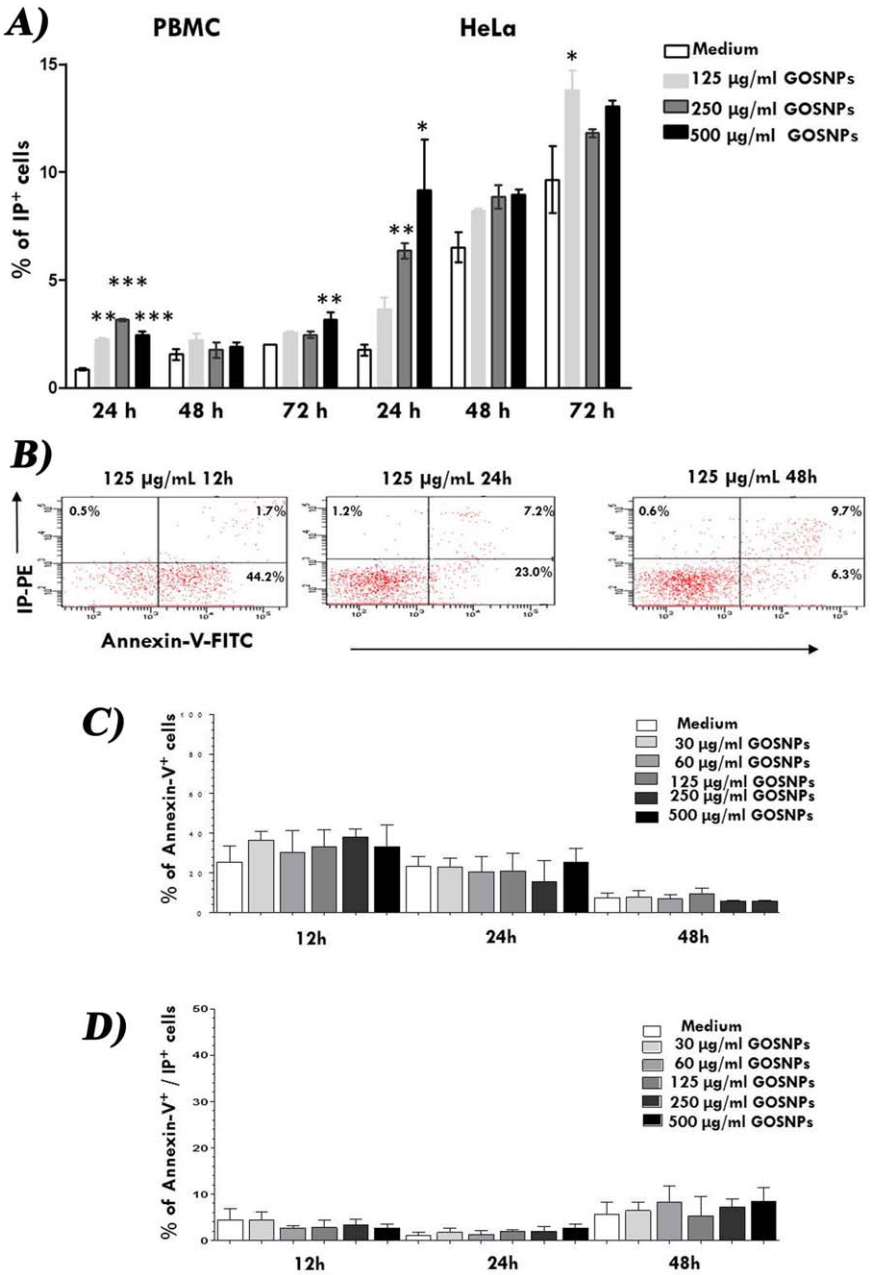

FIGURE 3. Cytotoxicity of GOSNPs. The effect of GOSNPs on the cytotoxicity was evaluated using flow cytometry. (A) PBMC and HeLa cells were incubated with or without GOSNPs for 24, 48, and 72 h. Positive cells to propidium iodide were used to show the cytotoxicity of the GOSNPs. Shown is the mean ± SE. $*p<0.05$, $**p<0.01$, $***p<0.001$ compared to the control cells (culture medium only). (B) Representative dot plots of flow cytometry of PBMC in the presence of 125 µg/mL of GOSNPs at 12, 24, and 48 h. The percentage of positive cells is shown in each quadrant. PBMC from three healthy donors were incubated with or without GOSNPs to final concentrations of 30, 60, 125, 250, or 500 µg/mL for 12, 24, and 48 h. (C) Results were expressed as the percentage of positive cells annexin-V+ (early apoptosis) or (D) double positive cells of annexin-V+ and IP+ (apoptosis and necrosis). All the experiments were repeated by triplicate.

nanomaterials have high photostability, no blinking, and extremely narrow emission peaks.[25]

In previous work, we have demonstrated that the ζ-potential of oxysulfide NPs in aqueous citrate or calcium carbonate buffered suspensions are in the range of −35 to −55 mV, thus denoting high colloid stability.[18] If we compared those results with this study, it is clear that cell culture medium strongly affects the surface charge distribution of oxysulfide nanoparticles. The variations in the particle charge observed in the culture media suggests that adsorption of proteins onto the particle surface is dominating the surface charge distribution.[26] On the other hand, the less-negative ζ-potential values obtained in cell culture media (Table I) indicate that electrostatic repulsion of the particles

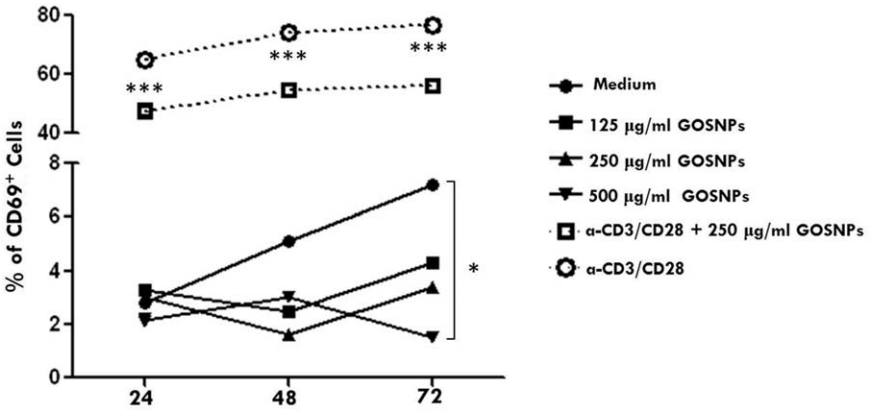

FIGURE 4. Immunomodulatory effect of GOSNPs on the CD69 expression. The effect of GOSNPs on the early cell activation antigen was evaluated using flow cytometry. PBMC were exposed to GOSNPs at final concentrations of 125, 250, or 500 μg/mL for 24, 48, and 72 h with or without the antibodies anti-CD3/CD28 used as stimuli. Cells in culture medium only were used as control. After each incubation time, cells were immunostained with anti-CD69-PE and analyzed using flow cytometry. Results were expressed as the percentage of CD69-positive cells. Experiments were performed in triplicate. $*p < 0.001$ compared to the control cells, and $***p < 0.001$ compared to the stimulated cells with anti-CD3/CD28.

diminishes, thus promoting collision and the growth of agglomerates that slowly precipitate in the suspensions.

To produce visible emission in the $G_2O_2S{:}Tb^{3+}$ matrix, the Gd^{3+} ion transfers nonradiative energy to the 4f levels of the Tb^{3+} ions, which rapidly produce populated levels of Tb^{3+}, relaxing to lower levels of energy. This produces an intense fluorescence emission between 400 and 600 nm.[27] In our case, the emission spectrum is mainly composed of three well-defined bands that are related to the radiative emission of the electronic 4f→5 days transitions of the Tb^{3+}

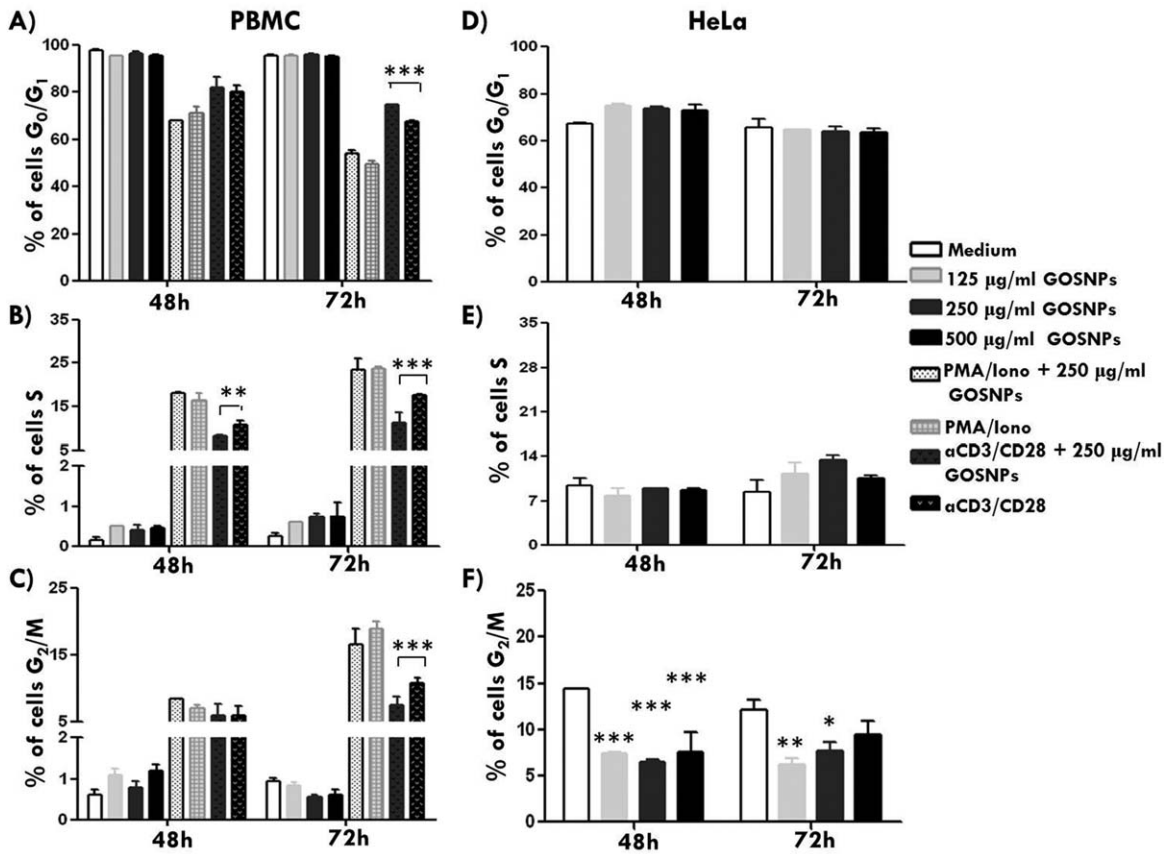

FIGURE 5. Immunomodulatory effect of GOSNPs on the cell cycle. The effect of GOSNPs on the cell cycle was evaluated using flow cytometry. PBMC were stimulated with 50 ng/mL PMA and 0.5 μg/mL ionomycin or anti-CD3/CD28 with and without GOSNP (final concentrations of 125, 250, or 500 μg/mL) for 24, 48, and 72 h. Cell nuclei were stained using PI and the nuclear DNA content was analyzed by flow cytometry. Results are expressed as the percentage of cells in distinct phases of the cell cycle: G0/G1 (normal diploid DNA), S- (DNA synthesis), and G2/M (mitosis) phases of the cell cycle. Additionally, HeLa cells were used and cultured only in the presence of GOSNPs for the same period of time described for PBMC. Shown is the mean ± SD of three independent experiments. $*p < 0.05$, $**p < 0.01$, $***p < 0.001$ compared to unstimulated cells (control).

ion. These bands are centered at 489, 544, and 584 nm, which are attributed to the transitions from the excitation level $^5D_4$ to the fundamental state ^7F_J ($J = 6$, 5, and 4) [Figure 1(D-IX)]. The most important emission at 544 nm corresponds to the green color of the electromagnetic spectrum, which is produced by the $^5D_4 \rightarrow {}^7F_5$ transition.[18]

It is widely accepted that the toxicity of NPs depends on physicochemical parameters such as particle size, shape, surface charge, surface chemistry, composition, and stability. Therefore, in this work, we have determined that negatively charged GOSNPs with spherical shape were internalized in normal cells, such as PBMC, and also in immortalized cells such as HeLa cells. We found that the uptake of GOSNPs in PBMC was more evident in a dose-dependent manner than that in the HeLa cells, where the uptake of GOSNPs was more significant at short times (6 h) and intermediate concentrations [Figure 2(I)]. These results show that there is a maximum GOSNP concentration that can be taken up by HeLa cells (250 μg/mL GOSNPs for 6 h). Thus, the decrease in the fluorescence observed at 48 and 72 h can be attributed to cellular proliferation. In this context, it has been reported that as a result of this division, the NPs are distributed in the daughter cells when the parental cells divide.[28]

The uptake mechanism of GOSNPs may vary depending on the cell type. However, research has shown that the adsorbed proteins on NPs determine particle uptake for various types of cells in the immune system and influence how NPs interact with other blood components.[29] Macromolecules or outside particles, such as NPs, might be internalized into the cell via membranous vesicles. This process is termed endocytosis and occurs by multiple mechanisms that fall into two broad categories, "phagocytosis" and "pinocytosis."[30] Phagocytosis is typically restricted to specialized cells, including macrophages, monocytes, and neutrophils, whereas pinocytosis occurs in all cells by at least four basic mechanisms: macropinocytosis, clathrin-mediated endocytosis, caveolae-mediated endocytosis, and clathrin- and caveolae-independent endocytosis.[30] It has been described that diverse proteins mediate the uptake of negatively charged NPs via phagocytosis through membrane receptors as scavenger or mannose receptors.[31,32] Therefore, due to the presence of these types of proteins in the culture medium, we suggest that one of these receptors might be involved in GOSNPs internalization by PBMC.[31] In the case of HeLa cells, the internalization of GOSNPs is related to pinocytosis and macropinocytosis mechanisms. In this respect, it has been reported that negatively charged particles are internalized by a caveloae-mediated pathway in epithelial cells like HeLa.[33] However, to confirm these hypotheses, it is necessary to determine the nature of proteins that are adsorbed on GOSNPs surface, or are involved in the caveolae-mediated mechanism. In addition, the two cells types used in this study are different. PMBC are primary immune cells freshly isolated from healthy donors and HeLa cells are cancer cells with an altered number of chromosomes and representative of a different tissue. In addition, these cells were incubated in different cell culture medium, which might have an influence on NP behavior. It has been reported that NPs affect the immune system and consequently human health. These effects may result from a unique set of physical characteristics and surface moieties. NPs are able to internalize into tissues and cells, and interact with proteins and DNA at a molecular level, producing direct or indirect effects on immune system modulation.[34]

Cytotoxicity analysis showed that more than 95% of the PBMC survived after incubation with GOSNPs at the highest concentration tested. In this regard, it has been reported that highly amino-functionalized fluorescent carbon NPs (proposed as potential materials for medical diagnostics and imaging) have a low cytotoxicity in A549 human lung adenocarcinoma epithelial cells,[35] whereas high cytotoxicity was measured when very high concentrations (>750 μg/mL) of Gd_2O_3:Tb^{3+} NPs were exposed to human skin fibroblast cells.[36] These results do not agree with our findings; however, it is important to note that we used different particle size and particle nature (for instance, oxysulfide instead of oxide). In this regard, the NPs exposed to PBMC used in our study showed low toxicity and excellent biocompatibility with potential application in healthy cells without side effects. It is noteworthy to mention that the percentage of IP+ or annexin-V+ cells was fluctuating and some sign of cytotoxicity was visible only at the shortest incubation time. The cytotoxicity observed could be related to the uptake of GOSNPs, which was dose dependent. In addition, with the annexin-V/IP assay, we could distinguish between necrotic and apoptotic cells.

On the other hand, the results of the toxicity on *Artemia* spp. are in agreement with those observed in the cytotoxic experiments above described. These results also resemble those found with TiO_2 NPs where NPs were not toxic at 24 h, but the mortality of nauplii increased toward 96 h exposure. This effect was attributed to the accumulation of particles inside the guts resulting in an impaired food uptake for a long time.[37]

Also, we evaluated the activation capacity of GOSNPs in PBMC using the activation marker CD69. The activation of lymphocytes and monocytes *in vitro* induces the expression of CD69. This molecule, which is one of the earliest inducible cell surface glycoproteins that is acquired during lymphoid activation, is involved in lymphocyte proliferation and functions as a signal-transmitting receptor in these cells.[38] Moreover, NPs such as polyglutamic acid are able to induce upregulation of co-stimulatory molecules on dendritic cells.[39] In contrast, our data shows that GOSNPs downregulate CD69 expression on the PBMC surface in all examined doses, which indicates that the GOSNPs may affect the activation of immune cells.

Alternatively, GOSNPs can induce cell-cycle arrest.[40] Here, we found that the cell cycle progression was directly affected by GOSNPs in HeLa cells. After 48 h of treatment, GOSNPs caused a significant decrease in the amount of cells in the G2/M phase compared to control cells. These latter results indicate that the GOSNP-treated cells can progress through the S phase into the G2 phase, where the cells accumulate [Figure 5(E,F)]. There can be several effects of GOSNPs on cell-cycle progression, including increased ROS production,[41] receptor-dependent Akt activation,[42] or the

upregulation of genes for cell-cycle progression.[43] In contrast to HeLa cells, cell-cycle arrest was only evident after stimulation in PBMC. Regardless of the mechanisms for cell-cycle arrest that was caused by GOSNPs, there is likely a link to the induction of apoptosis. Thus, apoptosis was more evident in HeLa cells than in PBMC (Figure 3). The concentration of GOSNPs used in this study may be high and their relevance in environmental and clinical settings needs to be evaluated in further studies.

In conclusion, our results demonstrate that GOSNPs are internalized, induce low levels of cytotoxicity, and modify the activation of normal human immune cells, but not HeLa cells. These results suggest that immune system cells are less sensitive to damage than are the cancer HeLa cells upon exposure to GOSNPs. The latter indicates that NP systems may be investigated for potential cancer therapy with reduced side effects. Then, this system might provide an alternative method to existing imaging methods because it has the additional advantage of allowing otherwise inaccessible measurements, such as MRI contrast enhancement and multimodal imaging, which can reveal new important biological information. Furthermore, the NPs' optical properties, photostability, high intensity emission, and absence of cytotoxicity make them suitable to replace organic dyes and QDs already reported in a great variety of applications.

ACKNOWLEDGMENTS

This work was supported by the CONACYT Projects CB-153161, and Infrastructure 225843; FAI C12-FAI-03-94.94. HAL and CEN received a fellowship from CONACYT, México (No. 270040 and No. 265938/217786). We thank Olga Davalos Montoya, Yatzil Alejandra Avalos Muñoz, and Alejandro Quintero González for technical support and Jeffrey Helm for helpful discussions.

REFERENCES

1. Schrand AM, Rahman MF, Hussain SM, Schlager JJ, Smith DA, Syed AF. Metal-based nanoparticles and their toxicity assessment. WIREs Nanomed Nanobiotechnol 2010;2:544–568.
2. Ahamed M, Alsalhi MS, Siddiqui MK. Silver nanoparticle applications and human health. Clin Chim Acta 2010;411:1841–1848.
3. Sanvicens N, Marco MP. Multifunctional nanoparticles properties and prospects for their use in human medicine. Trends Biotechnol 2008;26:425–433.
4. Gao J, Gu H, Xu B. Multifunctional magnetic nanoparticles: Design, synthesis, and biomedical applications. Acc Chem Res 2009;42:1097–1107.
5. Kelly KL, Coronado E, Zhao LL, Schatz GC: The optical properties of metal nanoparticles. The influence of size, shape, and dielectric environment. J Phys Chem B 2002;107:668–677.
6. Bouzigues C, Gacoin T, Alexandrou A. Biological applications of rare-earth based nanoparticles. ACS Nano 2011;5:8488–8505.
7. Sohaebuddin SK, Tang L. A simple method to visualize and assess the integrity of lysosomal membrane in mammalian cells using a fluorescent dye. Methods Mol Biol 2013;991:25–31. doi: 10.1007/978-1-62703-336-7_3.:25-31.
8. Resch-Genger U, Grabolle M, Cavaliere-Jaricot S, Nitschke R, Nann T. Quantum dots versus organic dyes as fluorescent labels. Nat Methods 2008;5:763–775.
9. Lewinski N, Colvin V, Drezek R. Cytotoxicity of nanoparticles. Small 2008;4:26–49.
10. Dobrovolskaia MA, Aggarwal P, Hall JB, McNeil SE: Preclinical studies to understand nanoparticle interaction with the immune system and its potential effects on nanoparticle biodistribution. Mol Pharm 2008;5:487–495.
11. Mendoza-Dorantes T, Pal U, Vega-Acosta JR, Marquez-Beltran C. Encapsulation and surface charge manipulation of organic and inorganic colloidal substrates by multilayered polyelectrolyte films. Colloids Surf A Physicochem Eng Asp 2013;434: 253–259.
12. Deok-Jung, Min KC, Sang ML, Kong MB, Phill GJ, Chi HL, Jae ML, Seungman Y, Ho KK, Seong SK, Jong SK. Flexible Gd2O2S:Tb scintillators pixelated with polyethylene microstructures for digital X-ray image sensors. J Micromech Microeng 2009;19:015014.
13. Guo H, Dong N, Yin M, Zhang W, Lou L, Xia S. Visible upconversion in rare earth ion-doped Gd2O3 nanocrystals. J Phys Chem B 2004;108:19205–19209.
14. Kim J, Kyoung Cha B, Hyung Bae J, Lee Ch, Kim H, Chang S, Cho G, Sim C, Kim T. Fabrication and characterization of pixelated Gd2O2S:Tb scintillator screens for digital X-ray imaging applications. Nucl Instrum Met Phys Res A 2011;633, Supplement 1:S303–S305.
15. Martin-Rodriguez R, Fischer S, Ivaturi A, Froehlich B, Kamer KW, Goldschmidt JC, Richards BS, Meijerink A. Highly efficient IR to NIR upconversion in Gd2O2S: Er3+ for photovoltaic applications. Chem Mater 2013;25:1912–1921.
16. Woo T, Kim T. Light collection enhancement of the digital X-ray detector using Gd2O2S:Tb and CsI:Tl phosphors in the aspect of nano-scale light dispersions. Radiat Phys Chem 2012;81:12–15.
17. Song Y, You H, Huang Y, Yang M, Zheng Y, Zhang L, Guo N. Highly uniform and monodisperse Gd2O2S:Ln3+ (Ln = Eu, Tb) submicrospheres: Solvothermal synthesis and luminescence properties. Inorg Chem 2010;49:11499–11504.
18. Hernandez-Adame L, Mendez-Blas A, Ruiz-Garcia J, Roger Vega-Acosta J, Medellin-Rodriguez FJ, Palestino G. Synthesis, characterization, and photoluminescence properties of Gd:Tb oxysulfide colloidal particles. Chem Eng J 2014;258:136–145.
19. Dispersion Technology. Dispersion Technology DT1200, Operating and Maintenance Manual. 2007, pp 1–235.
20. Bihari P, Vippola M, Schultes S, Praetner M, Khandoga A, Reichel C, Coester C, Tuomi T, Rehberg M, Krombach F. Optimized dispersion of nanoparticles for biological in vitro and in vivo studies. Particle Fibre Toxicol 2008;5:14.
21. Favre E, Thaler T. An engineering analysis of rotating sieves for hybridoma cell retention in stirred tank bioreactors. Cytotechnology 1992;9:11–19.
22. Maceo BM, Manns F, Borja D, Nankivil D, Uhlhorn S, Arrieta E, Ho A, Augusteyn RC, Parel JM. Contribution of the crystalline lens gradient refractive index to the accommodation amplitude in non-human primates: In vitro studies. J Vision 2011;11.
23. Xu Y, Tang H, Liu JH, Wang H, Liu Y. Evaluation of the adjuvant effect of silver nanoparticles both in vitro and in vivo. Toxicol Lett 2013;219:42–48.
24. Faucher MD, Morlotti R, Moune OK. The effects of added foreign ions in Gd2O2S: Tb3+; crystal field calculations, lifetimes, photo-luminescence and absorption spectra. J Lumines 2002;96: 37–49.
25. Cebim MA, Silva AAD, Davolos MR. Spectroscopy properties and energy level location of Gd2O2S:Pr3+,Ce3+. Phys Status Solidi (C) 2009;6:S171–S174.
26. Limbach LK, Li Y, Grass RN, Brunner TJ, Hintermann MA, Muller M, Gunther D, Stark WJ. Oxide nanoparticle uptake in human lung fibroblasts: Effects of particle size, agglomeration, and diffusion at low concentrations. Environ Sci Technol 2005;39: 9370–9376.
27. Debasu ML, Ananias D, Rocha J, Malta OL, Carlos LD. Energy-transfer from Gd(iii) to Tb(iii) in (Gd,Yb,Tb)PO4 nanocrystals. Phys Chem Chem Phys 2013;15:15565–15571.
28. Kim JA, Aberg C, Salvati A, Dawson KA: Role of cell cycle on the cellular uptake and dilution of nanoparticles in a cell population. Nat Nano 2012;7:62–68.
29. Dobrovolskaia MA, McNeil SE. Immunological properties of engineered nanomaterials. Nat Nano 2007;2:469–478.
30. Conner SD, Schmid SL. Regulated portals of entry into the cell. Nature 2003;422:37–44.
31. Nagayama S, Ogawara Ki, Minato K, Fukuoka Y, Takakura Y, Hashida M, Higaki K, Kimura T. Fetuin mediates hepatic uptake of

negatively charged nanoparticles via scavenger receptor. Int J Pharma 2007;329:192–198.
32. Gessner A, Lieske A, Paulke BR, Muller RH. Influence of surface charge density on protein adsorption on polymeric nanoparticles: Analysis by two-dimensional electrophoresis. Eur J Pharma Biopharma 2002;54:165–170.
33. Agarwal R, Singh V, Jurney P, Shi L, Sreenivasan SV, Roy K. Mammalian cells preferentially internalize hydrogel nanodiscs over nanorods and use shape-specific uptake mechanisms. Proc Natl Acad Sci 2013;110:17247–17252.
34. Chang C. The immune effects of naturally occurring and synthetic nanoparticles. J Autoimmun 2010;34:J234–J246.
35. Yang Y, Cui J, Zheng M, Hu C, Tan S, Xiao Y, Yang Q, Liu Y. One-step synthesis of amino-functionalized fluorescent carbon nanoparticles by hydrothermal carbonization of chitosan. Chem Commun (Camb) 2012;48:380–382.
36. Setyawati MI, Khoo PK, Eng BH, Xiong S, Zhao X, Das GK, Tan TT, Loo JS, Leong DT, Ng KW. Cytotoxic and genotoxic characterization of titanium dioxide, gadolinium oxide, and poly(lactic-co-glycolic acid) nanoparticles in human fibroblasts. J Biomed Mater Res A 2013;101:633–640.
37. Ates M, Daniels J, Arslan Z, Farah I. Effects of aqueous suspensions of titanium dioxide nanoparticles on Artemia salina: Assessment of nanoparticle aggregation, accumulation, and toxicity. Environ Monit Assess 2013;185:3339–3348.
38. Santis AG, Campanero MR, Alonso JL, Tugores A, Alonso MA, Yague E, Pivel JP, Sanchez-Madrid F. Tumor necrosis factor-alpha production induced in T lymphocytes through the AIM/CD69 activation pathway. Eur J Immunol 1992;22:1253–1259.
39. Takayuki Hamasaki, Tomofumi Uto, Takami Akagi, Mitsuru Akashi, Masanori Baba. Modulation of gene expression related to toll-like receptor signaling in dendritic cells by poly(γ-glutamic acid). Nanoparticles 2010. pp 748–756.
40. Thit A, Selck H, Bjerregaard HF: Toxicity of CuO nanoparticles and Cu ions to tight epithelial cells from *Xenopus laevis* (A6). Effects on proliferation, cell cycle progression and cell death. Toxicol In Vitro 2013;27:1596–1601.
41. Wang X, Tu Q, Zhao B, An Y, Wang JC, Liu W, Yuan MS, Ahmed SM, Xu J, Liu R, Zhang Y, Wang J. Effects of poly (L-lysine)-modified Fe3O4 nanoparticles on endogenous reactive oxygen species in cancer stem cells. Biomaterials 2013;34: 1155–1169.
42. Unfried K, Sydlik U, Bierhals K, Weissenberg A, Abel J. Carbon nanoparticle-induced lung epithelial cell proliferation is mediated by receptor-dependent Akt activation. Am J Physiol Lung Cell Mol Physiol 2008;294:L358–L367.
43. Asharani P, Sethu S, Lim HK, Balaji G, Valiyaveettil S, Hande MP. Differential regulation of intracellular factors mediating cell cycle, DNA repair and inflammation following exposure to silver nanoparticles in human cells. Genome Integr 2012;3:2−3.